

Silicon-based injection lasers using electronic intersubband transitions in the L valleys

Kristina Driscoll and Roberto Paiella^{a)}

Department of Electrical and Computer Engineering and Photonics Center, Boston University,
8 Saint Mary's Street, Boston, Massachusetts 02215

(Received 5 July 2006; accepted 24 September 2006; published online 8 November 2006)

The authors investigate the use of electronic intersubband transitions in Ge/SiGe quantum wells on SiGe (001) virtual substrates for the development of silicon-based long-wavelength quantum cascade lasers. These heterostructures can provide relatively strong quantum confinement in the Ge L valleys particularly if the SiGe layers are sufficiently thin so that L -to- Δ intervalley scattering paths are suppressed. Numerical simulations indicate that low-threshold operation can be obtained from these devices, thanks to the nonpolar nature of SiGe. Furthermore, the tensor properties of the L -valley effective mass are favorable for the development of vertical emitting intersubband lasers. © 2006 American Institute of Physics. [DOI: 10.1063/1.2385861]

The demonstration of Si-based injection lasers, which is complicated by the indirect band gap of silicon, has long been the subject of extensive research efforts, as it would enable the monolithic integration of electronic and photonic devices on an unprecedented scale. The use of intersubband (ISB) transitions in SiGe quantum cascade (QC) structures is a promising approach, since these transitions involve quantized states within a same band so that the nature of the band gap is irrelevant. Additionally, since SiGe alloys are nonpolar, they are particularly attractive for emission in the terahertz spectral region, where the use of III-V compounds is limited by their reststrahlen band. Recently, following various theoretical proposals,¹ ISB electroluminescence at mid- and far-infrared wavelengths has been demonstrated with SiGe quantum wells (QWs),²⁻⁴ although no subsequent report of laser action has yet appeared.

In all Si-based ISB devices considered so far hole ISB transitions have been employed, motivated by the generally larger valence-band offsets and/or smaller hole perpendicular effective masses of SiGe QWs, compared to the corresponding conduction-band properties. As a general rule,⁵⁻⁸ a compressively strained $\text{Si}_{1-x}\text{Ge}_x$ layer on a relaxed $\text{Si}_{1-z}\text{Ge}_z$ substrate (with $z < x$) provides an exceedingly small (~ 10 meV) conduction-band offset ΔE_c . A relatively large ΔE_c can be obtained in tensile strained SiGe wells; however, in such layers the conduction-band minimum occurs in the two Δ valleys along the growth direction ($\Delta 2$), whose large effective masses perpendicular to the QWs ($\sim 0.9m_0$) lead to exceedingly small ISB oscillator strengths. On the other hand, the development of hole ISB devices is hindered by the complexity of the valence-band structure. More importantly, achieving hole ISB population inversion is complicated by the presence of heavy-hole and mixed light-hole/split-off subbands at comparable energies, which leads to additional nonradiative decay channels.^{3,9}

In this letter we introduce and theoretically study SiGe QC lasers utilizing electronic ISB transitions in the L valleys, based on Ge/ $\text{Si}_{1-y}\text{Ge}_y$ QWs pseudomorphically grown on $\text{Si}_{1-z}\text{Ge}_z$ (001) virtual substrates with $z > y$. Although their overall conduction-band offset ΔE_c is in general rather small,

these QWs are nonetheless suitable for QC laser development due to the property illustrated in Fig. 1. The L -valley and $\Delta 2$ -valley conduction-band lineups individually consist of relatively deep QWs inverted relative to one another, i.e., while for the L -valley electrons Ge acts as the well material and $\text{Si}_{1-y}\text{Ge}_y$ as the barrier material, the opposite is true for the $\Delta 2$ -valley electrons.⁵⁻⁸ If the $\text{Si}_{1-y}\text{Ge}_y$ layers are thick relative to the electronic de Broglie wavelength (as in the barriers of most QW devices), the bound $\Delta 2$ states form a quasicontinuum as shown by the shaded areas in Fig. 1(a). Consequently, the excited L states in the Ge wells are extremely short lived due to intervalley scattering, and for all practical purposes electronic confinement in these wells is provided by the small offset ΔE_c . On the other hand, using very thin barriers (as those required in QC lasers for tunneling transport) leads to the situation illustrated in Fig. 1(b). In such cases, the $\text{Si}_{1-y}\text{Ge}_y$ layers support only one or a few $\Delta 2$ bound states well above the conduction-band minimum, and as a result the Ge QWs can confine L -valley electrons over an energy range much wider than ΔE_c .

The band lineups of these Ge/SiGe heterostructures can be computed using the results of several theoretical studies presented in the literature, e.g., Refs. 5–8. While some discrepancies exist among the predictions of these calculations, they all indicate that band offsets at the L -point ΔE_L well

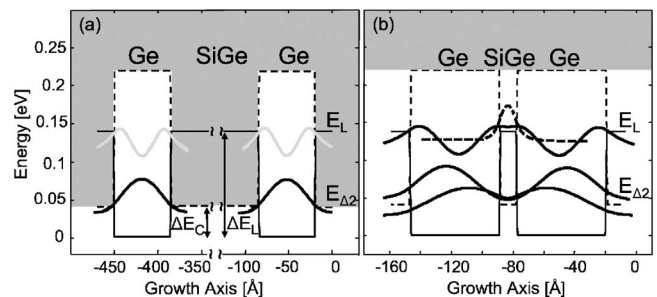


FIG. 1. Conduction-band profile and squared envelope functions of the quantized states of Ge/ $\text{Si}_{0.22}\text{Ge}_{0.78}$ QWs on a $\text{Si}_{0.12}\text{Ge}_{0.88}$ (001) virtual substrate, with (a) wide and (b) narrow $\text{Si}_{0.22}\text{Ge}_{0.78}$ barriers. The solid and dashed lines correspond to the L and $\Delta 2$ valleys, respectively; the light-gray solid lines denote L -valley bound states with very short lifetimes due to intervalley scattering; the shaded areas denote regions of (quasi) continuous $\Delta 2$ states.

^{a)}Electronic mail: rpaiella@bu.edu

above 100 meV and simultaneously overall offsets ΔE_c of a few tens of meV can be obtained with properly selected QW compositions. In this work we use the empirical model of Ref. 5 together with more recent values of the relevant material parameters.¹⁰ As shown in Fig. 1, this approach gives $\Delta E_L=138$ meV and $\Delta E_c=41$ meV for the exemplary case of Ge/Si_{0.22}Ge_{0.78} QWs on a Si_{0.12}Ge_{0.88} virtual substrate (the Γ and Δ_4 states lie at sufficiently higher energies that they can be ignored in this example).

While these values are fully appropriate for long-wavelength QC lasers, it should be mentioned that even larger barrier heights are predicted for similar QW systems in, e.g., Refs. 5–7. These discrepancies prevent us from estimating the shortest emission wavelength achievable with the proposed QC lasers, which is ultimately limited by ΔE_L . Additionally, they introduce some uncertainty in the design of the QC active material. Depending on which band-offset model is used, slightly different compositions and/or layer thicknesses are required to produce a given QC structure with a given set of bound states and resulting ISB gain spectrum. The structure presented below is meant to illustrate the large gain coefficients achievable with these devices; on the other hand, its exact implementation may require a more detailed experimental investigation of band offsets in Ge/SiGe QWs, and we believe that this work will provide a strong motivation for such a study.

We also point out that these QWs display a certain degree of strain compensation. Furthermore, despite their high Ge content, they are compatible with the standard Si(001) substrates of microelectronics, thanks to the availability of high quality SiGe virtual substrates grown on Si(001).⁷ In fact, Ge/SiGe QWs on Si(001) have already been used to demonstrate novel optoelectronic applications of silicon, such as the quantum-confined Stark effect.¹¹

Aside from the confinement energy, the other critical material parameter for QC lasers is the perpendicular effective mass, which should be as small as possible to yield large tunneling rates and oscillator strengths. In the QW system of Fig. 1, the constant-energy ellipsoids around the L -valley minima are tilted with respect to the (001) growth direction (z), giving rise to an inverse effective-mass tensor with both diagonal and off-diagonal nonzero terms. The relevant perpendicular effective mass is the diagonal term m_{zz} ,¹² which is related to the principal L -valley effective masses m_l and m_t according to¹³ $1/m_{zz}=2/(3m_l)+1/(3m_t)$. Using $m_l=0.08m_0$ and $m_t=1.59m_0$ for Ge,⁷ we obtain $m_{zz}=0.12m_0$, which is about three times smaller than the mass of the heavy holes used in the SiGe ISB emitters of Refs. 2–4.¹⁰ Furthermore, the nonzero off-diagonal terms $1/m_{xz}$ and $1/m_{yz}$ allow for coupling between the ISB electric dipoles (oriented along the growth axis) and in-plane polarized light.^{12,13} As a result, unlike traditional III–V QC lasers based on ISB transitions in the Γ minimum, these QWs provide ISB gain not only for TM but also for TE light, which is desirable for the development of vertically emitting devices.

Shown in Fig. 2 is an exemplary QC laser based on the QW system of Fig. 1, designed for emission near $42\ \mu\text{m}$ using the high-performance bound-to-continuum QC scheme.¹⁴ The solid (dashed) lines denote the conduction-band lineup and bound-state envelope functions for the L (Δ_2) valleys, computed with the effective-mass Schrödinger equation. The optical transitions occur between the L -valley states labeled $|4\rangle$ and $|3\rangle$ in each active region; the lower

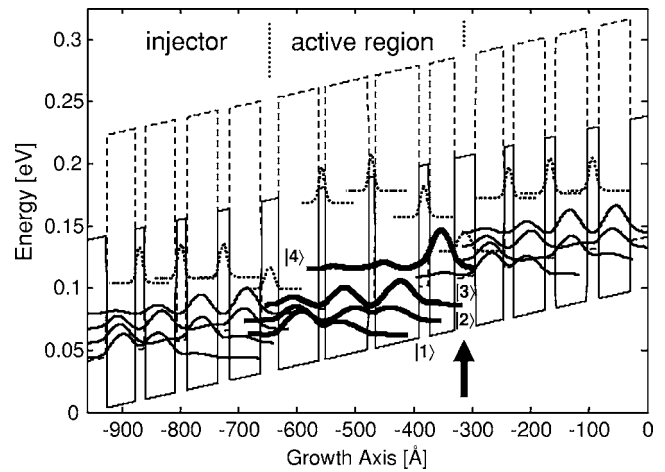


FIG. 2. Conduction-band profile and squared envelope functions of the relevant bound states of a QC laser based on the QW system of Fig. 1, in the presence of an external field of 11 kV/cm. The solid and dashed lines correspond to the L and Δ_2 valleys, respectively. The layer thicknesses of a single stage, starting from the injection barrier (indicated by the arrow) and moving downstream, are **36/43/17/76/11/74/11/69/30/54/20/54/18/53/17/49** (Å), where the bold numbers refer to barrier layers.

laser states $|3\rangle$ are rapidly depopulated through phonon-assisted scattering into states $|1\rangle$ and $|2\rangle$; and electrons are recycled from each active stage to the next through miniband transport in the injectors. Two design considerations, specific to the Ge/SiGe QW system, should be emphasized in relation to Fig. 2. First, for each Δ_2 bound state there must be a neighboring L state at lower energy; otherwise some of the injected electrons will be trapped in the Δ_2 valleys, leading to inefficient and possibly unstable transport into the laser states. Second, relatively diagonal laser transitions must be employed, i.e., with reduced overlap between the states $|3\rangle$ and $|4\rangle$, to ensure that the nonradiative decay time τ_{43} between these two states is long compared to the lifetime τ_3 of $|3\rangle$. In III–V QC lasers the dominant ISB scattering mechanism is the electron/LO-phonon polar interaction, whose resonant behavior allows one to engineer the relevant lifetimes through the ISB energy separations. In nonpolar SiGe alloys this interaction is absent and ISB relaxation is dominated by deformation-potential scattering,⁹ which does not exhibit any resonant behavior. Thus, the only design parameter available to control the scattering rate between two subbands is their envelope-function overlap.

As a figure of merit for the performance of this device, we have computed its material gain coefficient for TE and TM light using the following expression derived from a standard rate-equation model of QC lasers:¹⁴

$$g_{\text{TE,TM}} = \frac{\hbar q^2}{\varepsilon_0 c m_0} \frac{\eta f_{\text{TE,TM}}}{n \gamma L_p} \left[\tau_4 \left(1 - \frac{\tau_3}{\tau_{43}} \right) \frac{J}{q} - N_d e^{-\Delta/k_B T} \right]. \quad (1)$$

Here n is the refractive index, γ the full width at half maximum (FWHM) of the laser transition, L_p the length of one period of the active material, η the injection efficiency, J the current density, N_d the donor sheet density per period, and Δ the energy separation between each lower laser state $|3\rangle$ and the quasi-Fermi level of the injector downstream. Finally, the oscillator strength of the laser transition is given by $f_{\text{TE,TM}} = (2m_0 \langle 3|p_z|4\rangle^2) / (m_{xz,zz}^2 (E_4 - E_3))$, where \mathbf{p} is the momentum operator.¹² Using the aforementioned value of m_{zz} and

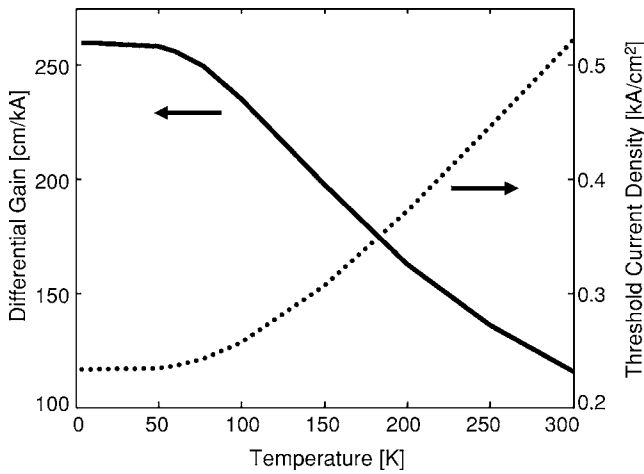


FIG. 3. Calculated differential gain coefficient dg_{TM}/dJ (solid line) and threshold current density J_{th} (dotted line) of the QC laser of Fig. 2 vs temperature.

$1/m_{xz} = 1/(3m_t) - 1/(3m_l) = 1/(0.26m_0)$, a non-negligible TE-to-TM gain ratio $g_{\text{TE}}/g_{\text{TM}} = (m_{zz}/m_{xz})^2 = 0.21$ is obtained.^{12,13}

To model intravalley deformation-potential scattering, the following expressions can be used for the transition rates between subbands $|i\rangle$ and $|f\rangle$ due to emission (upper sign) and absorption (lower sign) of optical and acoustic phonons, respectively:¹⁵

$$\frac{1}{\tau_{\text{opt}}^{\pm}} = \frac{D_0^2 m^* G}{4\pi\hbar^2 \rho \omega_0} \left(n(\omega_0) + \frac{1}{2} \pm \frac{1}{2} \right) H(E_i - E_f \mp \hbar\omega_0), \quad (2)$$

$$\frac{1}{\tau_{\text{ac}}^{\pm}} = \frac{\Xi^2 k_B T m^* G}{4\pi\hbar^3 \rho v_s^2} H(E_i - E_f). \quad (3)$$

Here D_0 and Ξ are the optical and acoustic deformation potentials, taken to be scalar for simplicity, ω_0 and $n(\omega_0)$ are the $\mathbf{q}=0$ optical phonon frequency and equilibrium number, m^* is the two-dimensional density-of-states effective mass, ρ is the mass density, v_s is the sound velocity, H is the step function, and $G = \int dq_z |f| e^{iq_z z} |i\rangle|^2$. Regarding intervalley scattering, it can be treated with a phenomenological model which includes the contributions of optical and acoustic phonons in a single expression.¹⁶ In this approach Eq. (2) is used for the L -to- Δ_2 (L -to- L) intervalley scattering rates, with D_0 and ω_0 replaced by model parameters $D_{L\Delta_2}$ and $\omega_{L\Delta_2}$ (D_{LL} and ω_{LL}) extrapolated from experimental data.

For the simulations presented below, we used material parameters of Ge as appropriate to the high Ge content of the QC gain medium of Fig. 2. These parameters were taken from Refs. 7 and 16 and are as follows: $D_0 = 3.5 \times 10^8$ eV/cm, $\Xi = 2.5$ eV, $\hbar\omega_0 = 37$ meV, $m_L^* = 0.15m_0$, $m_{\Delta_2}^* = 0.19m_0$, $\rho = 5.32$ g/cm³, $v_s = 3.9 \times 10^5$ cm/s, $D_{LL} = 5.26 \times 10^8$ eV/cm, $D_{L\Delta_2} = 4.65 \times 10^8$ eV/cm, $\hbar\omega_{LL} = 24$ meV, $\hbar\omega_{L\Delta_2} = 23$ meV, and $n = 3.97$. The lifetimes τ_3 and τ_4 were computed using Eqs. (2) and (3), including contributions

from all lower-lying subbands in all valleys. Exemplary values are $\tau_3 = 9.2$ ps, $\tau_4 = 13.6$ ps, and $\tau_{43} = 35.5$ ps at room temperature, which are relatively long, thanks to the nonpolar nature of SiGe alloys. Finally, in Eq. (1) we used a conservative value of $\gamma = 10$ meV for the laser transition FWHM, a typical doping density for long-wavelength QC lasers $N_d = 5 \times 10^{10}$ cm⁻², and unit injection efficiency $\eta = 1$.

The solid line in Fig. 3 is the calculated TM differential gain dg_{TM}/dJ of the QC laser of Fig. 2 plotted versus temperature. Relatively large values of over 115 cm/kA are obtained up to room temperature, suggesting that low-threshold operation can be achieved. To illustrate, we have computed the threshold current density from the relation $\Gamma g(J_{\text{th}}) = \alpha_w + \alpha_m$ assuming a typical cavity length of 1 mm (giving a mirror loss $\alpha_m \approx 10$ cm⁻¹), a waveguide loss $\alpha_w \approx 20$ cm⁻¹, and a confinement factor $\Gamma \approx 0.5$; the latter two parameters were taken from a recent theoretical study of surface-plasmon waveguides for SiGe QC lasers at similar wavelengths (35 μm).¹⁷ As shown by the dotted line in Fig. 3, the resulting threshold current density ranges from 0.23 kA/cm² at 10 K to 0.52 kA/cm² at 300 K. These values are on par with those of existing III-V terahertz QC lasers, and thus substantiate the potential of the QW system of Fig. 1 for the development of injection lasers fully compatible with Si(001) technology. Such devices are suitable to cover a very wide spectral range in the far infrared due to the lack of reststrahlen band in SiGe. Additionally, the presence of significant TE gain is attractive for the development of vertical emitting QC lasers.

- ¹G. Sun, L. Friedman, and R. A. Soref, Appl. Phys. Lett. **66**, 3425 (1995).
- ²G. Dehlinger, L. Diehl, U. Gennser, H. Sigg, J. Faist, K. Ensslin, D. Grützmacher, and E. Müller, Science **290**, 2277 (2000).
- ³I. Bormann, K. Brunner, S. Hackenbuchner, G. Zandler, G. Abstreiter, S. Schmult, and W. Wegscheider, Appl. Phys. Lett. **80**, 2260 (2002).
- ⁴S. A. Lynch, R. Bates, D. J. Paul, D. J. Norris, A. G. Cullis, Z. Ikončić, R. W. Kelsall, P. Harrison, D. D. Arnone, and C. R. Pidgeon, Appl. Phys. Lett. **81**, 1543 (2002).
- ⁵C. G. Van de Walle and R. M. Martin, Phys. Rev. B **34**, 5621 (1986).
- ⁶M. M. Rieger and P. Vogl, Phys. Rev. B **48**, 14276 (1993).
- ⁷F. Schäffler, Semicond. Sci. Technol. **12**, 1515 (1997).
- ⁸S. Galdin, P. Dollfus, V. Aubry-Fortuna, P. Hesto, and H. J. Osten, Semicond. Sci. Technol. **15**, 565 (2000).
- ⁹K. Reimann, R. A. Kaindl, and M. Woerner, Phys. Rev. B **65**, 045302 (2001).
- ¹⁰L. Yang, J. R. Watling, R. C. W. Wilkins, M. Borici, J. R. Barker, A. Asenov, and S. Roy, Semicond. Sci. Technol. **19**, 1174 (2004).
- ¹¹Y.-H. Kuo, Y. K. Lee, Y. Ge, S. Ren, J. E. Roth, T. I. Kamins, D. A. B. Miller, and J. S. Harris, Nature (London) **437**, 1334 (2005).
- ¹²S. K. Chun and K. L. Wang, Phys. Rev. B **46**, 7682 (1992).
- ¹³W. Xu, Y. Fu, and M. Willander, Phys. Rev. B **49**, 13760 (1994).
- ¹⁴C. Sirtori and R. Teissier, in *Intersubband Transitions in Quantum Structures*, edited by R. Paiella (McGraw-Hill, New York, 2006), Chap. 1.
- ¹⁵B. K. Ridley, *Electrons and Phonons in Semiconductor Multilayers* (Cambridge University Press, Cambridge, 1997), Chap. 1.
- ¹⁶M. V. Fischetti, IEEE Trans. Electron Devices **38**, 634 (1991).
- ¹⁷Z. Ikončić, R. W. Kelsall, and P. Harrison, Semicond. Sci. Technol. **19**, 76 (2004).